Stable Cation Inversion at the $MgAl_2O_4(100)$ Surface

Morten K. Rasmussen,[1] Adam S. Foster,[2,3] Berit Hinnemann,[4] Filippo F. Canova,[2,3] Stig Helveg,[4] Kristoffer Meinander,[1] Natalia M. Martin,[5] Jan Knudsen,[5] Alina Vlad,[6] Edvin Lundgren,[5] Andreas Stierle,[6] Flemming Besenbacher,[1] and Jeppe V. Lauritsen[1]

[1]*Interdisciplinary Nanoscience Center (iNANO), Aarhus University, Aarhus, Denmark*
[2]*Department of Physics, Tampere University of Technology, Tampere, Finland*
[3]*Department of Applied Physics, Aalto University School of Science and Technology, Helsinki, Finland*
[4]*Haldor Topsøe A/S, Nymøllevej 55, Kgs. Lyngby, Denmark*
[5]*Division of Synchrotron Radiation Research, Institute of Physics, Lund University, Lund, Sweden*
[6]*Max-Planck-Institut für Metallforschung, Heisenbergstraße 3, Stuttgart, Germany*

(Received 21 March 2011; published 13 July 2011)

From an interplay of atom-resolved noncontact atomic force microscopy, surface x-ray diffraction experiments, and density functional theory calculations, we reveal the detailed atomic-scale structure of the (100) surface of an insulating ternary metal oxide, $MgAl_2O_4$ (spinel). We surprisingly find that the $MgAl_2O_4(100)$ surface is terminated by an Al and O-rich structure with a thermodynamically favored amount of Al atoms interchanged with Mg. This finding implies that so-called Mg-Al antisites, which are defects in the bulk of $MgAl_2O_4$, become a thermodynamically stable and integral part of the surface.

DOI: 10.1103/PhysRevLett.107.036102 PACS numbers: 68.47.Gh, 68.35.Md, 68.37.Ps, 68.49.Uv

Metal oxide spinels are very interesting materials both from a fundamental and an applied point of view. They are used industrially in ceramics technology, materials science, and in catalysis [1–3]. They belong to the class of insulating oxides, the surface structure of which has basically remained unsolved because many of the traditional surface science techniques are hampered by charging. Using the complementary direct atomic-scale and crystallographic reciprocal space information obtained by noncontact atomic force microscopy (NC-AFM) [4–7] and surface x-ray diffraction (SXRD), together with density functional theory (DFT) structure calculations and NC-AFM simulations, we present in this study the first detailed model of the atomic arrangement and prevalent defects on the (100) surface of $MgAl_2O_4$.

$MgAl_2O_4$ adopts the normal spinel structure [Fig. 1(a)] described by a slightly deformed cubic lattice of oxygen atoms with Mg^{2+} occupying 1/8 of the tetrahedral holes and Al^{3+} occupying 1/2 of the octahedral holes. A well-known and important defect in spinel is the Mg-Al antisite, formed by a pairwise interchange and trapping of the Mg and Al cations [8]. However, it has remained unclear to what extent such defects could be important at the surface. $MgAl_2O_4$ surfaces formed by cleavage along the low-index planes are polar [9] and, consequently, only surfaces stabilized by removing a significant amount of the surface atoms have been found in theoretical models [10,11]. In contrast, our results unambiguously show that the $MgAl_2O_4(100)$ surface is terminated by an intact Al and O-terminated structure, which, in the thermodynamically stable configuration, exposes a significant number of surface Mg-Al antisite defects.

The $MgAl_2O_4(100)$ surface was prepared by ion bombardment and annealing to 1400 K in 10^{-7} mbar O_2. The NC-AFM experiments were performed in ultrahigh vacuum (UHV, $P < 1 \times 10^{-10}$ mbar) using an Omicron VT-AFM/STM. The NC-AFM measurements were performed by oscillating a silicon cantilever with constant amplitude and measuring the frequency shift (df) [12]. The SXRD experiments were performed at the MPI-MF beam line at the Angstrom Quelle Karlsruhe. The program package ROD [13] was used for fitting the structure factors. DFT calculations were performed using the DACAPO code (see [12] for details). For the surface energy plots we use the chemical potential formalism [14]. The calculations of the tip-surface interaction for NC-AFM simulations were performed using the periodic plane-wave basis VASP code [15], implementing the spin-polarized DFT and the generalized gradient approximation (see [12] for details).

After preparation we obtain a flat $MgAl_2O_4(100)$ surface which is interrupted by a few nanometer wide square pits that cover 20%–30% of the surface (Fig. S1 in [12]). As illustrated in the side view ball model of Fig. 1(a), the repetition unit in the ⟨100⟩ direction reflects a [Mg_2-O_4-Al_4-O_4] stacking with a 2.02 Å separation distance between such stacks,

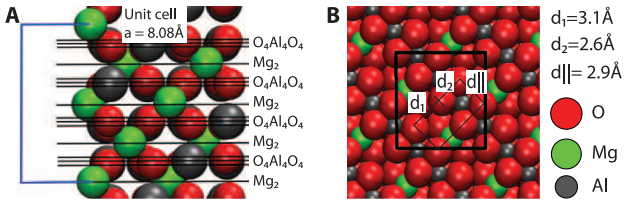

FIG. 1 (color). (A) Side view ball model of the bulk unit cell of normal $MgAl_2O_4$ spinel. (b) Top view ball model showing the structure of the experimentally observed O_4-Al_4-O_4 terminated surface.

which is consistent with the step height and hole depths measured from the NC-AFM topographs determined to be 2.0 ± 0.1 Å (or multiples thereof). Two types of (100) surface terminations can be obtained from a bulk truncation of $MgAl_2O_4$ which results in the fully Mg-terminated surface or a O_4-Al_4-O_4 termination exposing O and Al atoms [Fig. 1(b)], respectively. These surfaces are polar, but a nonpolar, stoichiometric surface termination may exist for a surface with vacancies, e.g., when the Mg_2 layer is instead split between two surfaces leading to a 50% Mg-vacancy concentration on the Mg-terminated surface [12]. Similarly for the Al_4 termination, nonpolar surfaces with vacancies are created [12], but these generally have high surface energies [10,11]. Surprisingly, however, the atom-resolved NC-AFM results in Figs. 2(a) and 2(b) reveal that the $MgAl_2O_4(100)$ surface has a rather modest number of defects in a surface which otherwise reflects the intact O_4-Al_4-O_4 structure.

Despite the fact that the two NC-AFM images in Figs. 2(a) and 2(b) have a different appearance, they are complementary NC-AFM images of the same surface revealing the anion and cation sublattice of the surface, respectively. This finding is explained by the fact that short-range atomic forces, acting between the AFM tip and the $MgAl_2O_4(100)$ surface, may be dominated by electrostatic forces, and that the NC-AFM atomic contrast then depends strongly on the chemical specificity of the AFM tip-apex atom [16–18]. Specifically, a positively terminated tip apex (e.g., Mg) created during a tip-surface contact preferentially interacts attractively with the negative O atoms in the $MgAl_2O_4(100)$ surface and therefore yields a high NC-AFM contrast on these sites, or vice versa, an electronegative O tip atom interacts more strongly with the cations on the surface. This distinct NC-AFM contrast is fully reproduced in our NC-AFM simulations of the relevant $MgAl_2O_4(100)$ surface. The simulations are performed by a calculation of the short-range tip-surface interaction forces between the $MgAl_2O_4(100)$ surface and a MgO nanocluster model tip [12,19], which is terminated by either a positive Mg^{2+} or negative O^{2-} ion. The NC-AFM image in Fig. 2(a) and the corresponding simulated image in Fig. 2(c) of the O_4-Al_4-O_4 termination both reveal an unambiguous double row structure consisting of protrusions resolved with an interatomic distance along the row of 2.8 ± 0.1 Å. As illustrated in the top view ball model in Fig. 1(b), the O_4-Al_4-O_4 termination of $MgAl_2O_4(100)$ is indeed characterized by rows of Al atoms (gray) each coordinated to four surface O atoms (red), which form the same double row structure with a $d_{\|} = 2.9$ Å periodicity. We therefore conclude that the NC-AFM image in Fig. 2(a) reflects a situation where the sublattice of O^{2-} atoms in the O_4-Al_4-O_4 termination is imaged with an electropositive tip apex. In the complementary NC-AFM image in Fig. 2(b), only a single row structure is revealed. This is again fully reproduced in the simulated image [Fig. 2(d)] which is therefore, in a corresponding way, attributed to a NC-AFM image recorded with an electronegative tip apex and where the single row structure now reflects the position of Al^{3+} atoms.

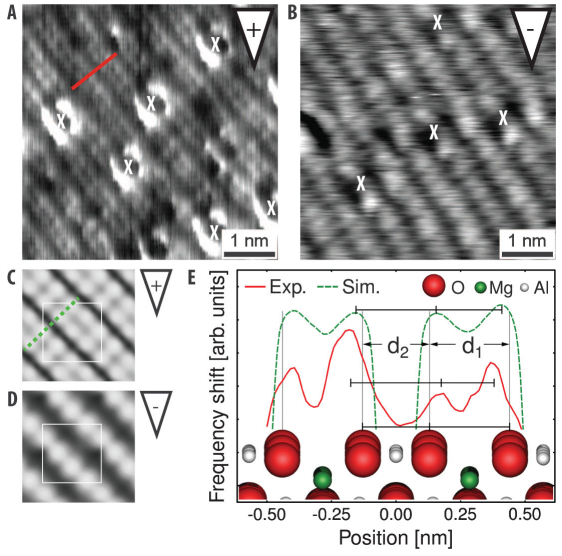

FIG. 2 (color). NC-AFM images of the $MgAl_2O_4(100)$ surface recorded in constant height mode with a contrast reflecting (a) a positively charged tip apex and (b) negatively charged tip apex. Imaging condition for (a) is $df_{set} = -126$ Hz, $U_{bias} = 1.0$ V, $A_{p\text{-}p} = 10$ nm and for (b) is $df_{set} = -30$ Hz, $U_{bias} = 3.0$ V, $A_{p\text{-}p} = 10$ nm. (c) Positive and (d) negative tip NC-AFM simulation of the O_4-Al_4-O_4 surface. (e) Comparison of an experimental line scan with a line scan simulated with a positive tip.

SXRD also reveals the presence of an unreconstructed $MgAl_2O_4(100)$ surface terminated by the O_4-Al_4-O_4 layer. The absence of fractional order spots when scanning the (h, k) space for fixed l values rules out reconstructions arising from ordered vacancy patterns such as the 50% Mg-terminated surface, and among the bulk-terminated solutions the initial fit of the x-ray data yielded the lowest χ^2 value ([12]) for O_4-Al_4-O_4. During further refinement of the structural model for O_4-Al_4-O_4, atomic displacements and the occupation probability of the atoms in the topmost layers were allowed to vary. The SXRD data are represented in Fig. 3(a) by the characteristic crystal-truncation-rod (CTR) scans (open and filled circles), which reflect linear regions in momentum space normal to the surface, together with the best fit of the CTR scans (full lines) for the structural model of the O_4-Al_4-O_4 termination [Figs. 3(b) and 3(c)]. We find that the overall atomic displacements from their bulk positions are surprisingly small (< 0.12 Å). An exception is the distance between the oxygen atoms across the double row structure (d_2), which on average is decreased by 0.20 Å to 2.39 Å. These observations are in very good agreement with the results from DFT calculations that predict a distance of 2.28 and 2.43 Å with or without a Mg neighbor, respectively. Furthermore, we find occupancies in the topmost layer for O (0.70), Al (0.61), and Mg (0.55) [Fig. 3(d)] relative to an ideal, stoichiometric $MgAl_2O_4(100)$ surface,

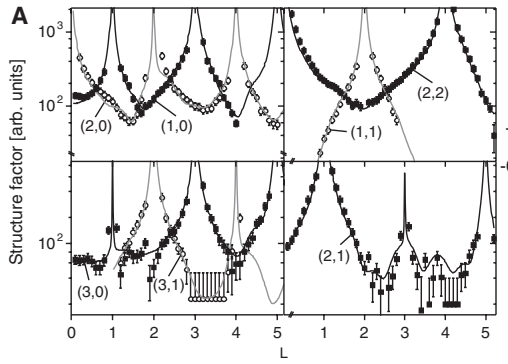

stack	element	occupancy
1	O/Al	0.70/0.61
	Mg	0.55
2	O/Al	0.92/0.71
	Mg	0.74
3	O/Al	0.96/0.96
	Mg	1.0
4	O/Al	1.0/0.89
	Mg	0.96

FIG. 3 (color). (a) X-ray structure factors from the clean $MgAl_2O_4(100)$ surface (open and filled circles). The solid lines represent best fits to the data according to the structural model. Ball models of the SXRD refined structure (b) along the [100] and (c) along the [010] directions. (d) Table with occupancies for the top four layers (relative to the extended ideal flat surface) obtained from the SXRD data.

which could indicate the presence of a significant amount of both cation and anion vacancies, in apparent conflict with the atom-resolved NC-AFM images. The reduced occupancies can, however, be explained by regular nanometer sized pits on the surface (Fig. S1 in [12]), which can be regarded as vacancy islands corresponding to a missing Mg_2-O_4-Al_4-O_4 layer. Assuming an O and Al termination at the pit edges, the size and the pit coverage of 30% observed with NC-AFM corresponds exactly to the relative concentrations of O, Al, and Mg derived from SXRD. For the three lower-lying $MgAl_2O_4(100)$ layers, the SXRD fits also show that the occupancy is gradually increased toward unity [Fig. 3(d)], consistent with the up to 4 layers deep square pits observed in the NC-AFM images.

To understand the surprising stability of the O_4-Al_4-O_4 surface termination we have performed extensive DFT calculations of the relevant $MgAl_2O_4(100)$ surface terminations. In agreement with previous calculations carried out without the influence of any adsorbing gases [10,11], calculations first show that the 50% Mg-terminated surface is most stable. However, for an open system reflecting the experimental conditions, several other surface terminations, which do not keep the full stoichiometry, become more stable. In particular, the experimentally observed O_4-Al_4-O_4 terminated surface gains stability compared to the Mg-termination surface when the experimental conditions are taken into consideration, i.e., when hydrogen and oxygen adsorb on the surface. Figure 4(a) shows a surface energy diagram of the $MgAl_2O_4(100)$ surface as a function of temperature at a fixed pressure of oxygen (1×10^{-7} mbar) and residual pressure of hydrogen (1×10^{-10} mbar). Adsorption of both one and two H per unit cell on any of the O atoms of the clean O_4-Al_4-O_4 terminated surface is very favorable (see Fig. S4 in [12]). Figure 4(c) illustrates the most stable structure found for adsorption of two H (O_4-Al_4-O_4-2H), which has an adsorption energy of -2.75 eV per H. A coverage of four H per unit cell was less stable, but becomes favored at low temperatures due to the entropy term [Fig. 4(a)]. The O_4-Al_4-O_4 structure with H adsorbed is thus favored even under clean UHV conditions except at a very high temperature. Calculated force-distance curves show that H causes a small perturbation in force interactions around the oxygen on the O_4-Al_4-O_4 surface in the positive tip NC-AFM images, but the narrow energy range adopted by the H among the different adsorption configurations suggests a high mobility on the surface, which may explain why no static features directly attributable to H can be identified in Fig. 2(a).

Very interestingly, the atom-resolved NC-AFM images of the O_4-Al_4-O_4 termination also directly reveal a number of lattice point defects in both NC-AFM imaging modes in Figs. 2(a) and 2(b). The density is $\sim$0.15 per surface unit cell in both modes reflecting that the defects originate from the same lattice point defect. In the NC-AFM image recorded with an electronegative tip [Fig. 2(b)], the defects are imaged as a hole which is centered directly on the bright row of protrusion defined by the Al lattice of the O_4-Al_4-O_4 termination. On the other hand, for the NC-AFM image recorded with an electropositive tip [Fig. 2(a)], the defect is located on the darkest rows and appears as a hole surrounded by a bright region on both sides. As depicted from the simulated NC-AFM line scan in Fig. 2(e), due to the domination of the electrostatic forces, the row with the darkest contrast (strongest repulsive interaction) is in fact directly over the Al sites whereas the strongest attractive interaction (brightest contrast) is in a slightly shifted position between the O atoms. The defects are therefore also in this image located on the Al lattice. The shift in the apparent position of the bright protrusion in the NC-AFM line scan compared to the O site is explained by the asymmetry experienced by the tip as it scans the surface, where the neighboring Al^{3+} screens the negative charge more efficiently compared to the Mg^{2+} located deeper in the surface. As tentative candidates for the defect located on Al sites of the O_4-Al_4-O_4 terminated surface, we have considered both Al vacancies and Mg-Al antisite defects formed by cation inversion between subsurface Mg and Al. In both cases the electrostatic map of the surface is strongly modified, and such sites are therefore

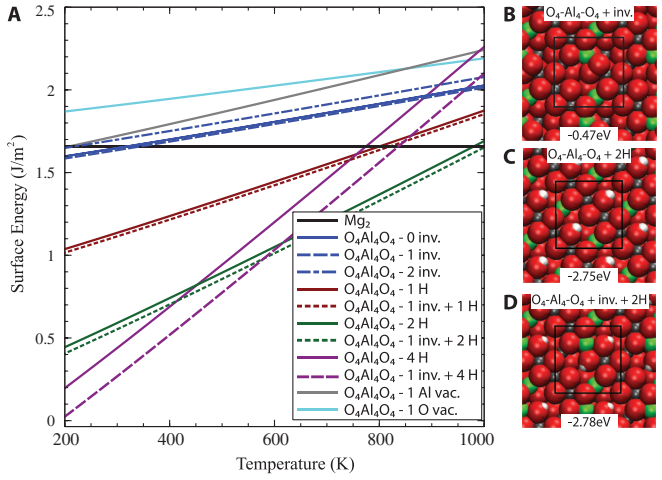

FIG. 4 (color). (a) Surface energy plot of the most relevant surfaces with or without cation inversion (inv.) and H adsorption, obtained from the DFT calculations using the chemical potential formalism. The plot reflects the stability in terms of the surface energy of the relevant phases at the experimental preparation conditions [$P(O_2) = 1 \times 10^{-7}$ mbar and $P(H_2) = 1 \times 10^{-10}$ mbar] as a function of temperature. Top view ball models of the O_4-Al_4-O_4 terminated $MgAl_2O_4(100)$ surface with (b) one antisite per unit cell, (c) most stable configuration at saturation coverage of 2H per unit cell on plain O_4-Al_4-O_4, and (d) most stable configuration at saturation coverage of 2H per unit cell on the O_4-Al_4-O_4 surface with one antisite (overall most stable configuration).

extremely sensitive to NC-AFM imaging with a charged tip [18]. Force-distance curves calculated above the Al vacancy or the Mg-Al antisite qualitatively verify that the contrast is reduced as seen in the experiment [Fig. 2(b)]. DFT calculations, however, surprisingly show that one Mg-Al inversion per unit cell is energetically much more favorable with a formation energy of -0.47 eV, whereas formation of one Al vacancy is very unfavorable over the entire temperature range [Fig. 4(a)]. This strongly suggests that the defects observed are Mg-Al antisites which act to stabilize the O_4-Al_4-O_4 terminated surface in surprising contrast to bulk cation inversion which is strongly endothermic [20]. Formation of more than one Mg-Al antisite within a single unit cell was found unfavorable [12], which is in agreement with the NC-AFM data [Figs. 2(a) and 2(b)] where the Mg-Al antisites are always spaced apart. For comparison we also investigated cation inversion on the 50% Mg-terminated surface, and although antisite formation is also favorable on this surface, such surfaces were overall less stable and not observed experimentally. DFT calculations show that adsorption of two [Fig. 4(d)] and up to four H atoms per unit cell on the inverted surface increases the stability with similar adsorption energies as for the noninverted surface. The thermodynamic model thus shows that the O_4-Al_4-O_4 surface with Mg-Al antisites and OH groups is stable under nearly all O_2 and H_2 containing conditions.

A fundamental new finding is that Mg-Al antisites are a natural part of the $MgAl_2O_4$ surface and not a kinetically trapped "defect" like in the bulk. The favorable cation inversion is driven by the need to rearrange charges in the surface layer to compensate the surface polarity. Cation inversion thus redistributes a substantial amount of the cations in the spinel surface and places Mg atoms in both an octahedral-like coordination to the O and the Al atoms in a tetrahedral environment. The coordination of O at the surface is known to strongly affect the adsorption properties of metal oxide surfaces in general and previous IR-spectroscopy studies have indeed provided evidence for Brønsted acid-base properties, reflecting both Al and Mg sites in $MgAl_2O_4$ spinel powders [21]. We anticipate that the surface reconstruction by cation inversion may be present also for the other polar facets of $MgAl_2O_4$ and suggest that it is a general phenomenon for spinel structures, since NMR spectroscopy studies have indeed shown that the degree of cation inversion may scale with the surface area of some metal oxide spinel powders [22].

[1] J. L. G. Fierro, *Metal Oxides—Chemistry and Applications* (Taylor and Francis, Boca Raton, FL, 2006).
[2] J. R. Rostrup-Nielsen, *Catalysis—Science and Technology* (Springer-Verlag, Berlin, 1984), Vol. 5, pp. 1–130.
[3] S. D. Jackson, *Metal Oxide Catalysis* (Wiley-VCH Verlag GmbH & Co., Weinheim, 2009), Vol. 2, p. 485.
[4] S. Morita *et al.*, *Noncontact Atomic Force Microscopy* (Springer, Berlin, 2009), Vol. 2, p. 307.
[5] J. V. Lauritsen *et al.*, J. Phys. Condens. Matter **22**, 263001 (2010).
[6] C. Barth *et al.*, Adv. Mater. **23**, 477 (2011).
[7] E. I. Altman *et al.*, Adv. Mater. **22**, 2854 (2010).
[8] K. E. Sickafus *et al.*, J. Am. Ceram. Soc. **82**, 3279 (1999).
[9] J. Goniakowski *et al.*, Rep. Prog. Phys. **71**, 016501 (2008).
[10] C. M. Fang *et al.*, J. Am. Ceram. Soc. **83**, 2082 (2000).
[11] M. J. Davies *et al.*, J. Mater. Chem. **4**, 813 (1994).
[12] See Supplemental Material at http://link.aps.org/supplemental/10.1103/PhysRevLett.107.036102 for the methods section and supporting DFT calculations.
[13] E. Vlieg, J. Appl. Crystallogr. **33**, 401 (2000).
[14] K. Reuter and M. Scheffler, Phys. Rev. Lett. **90**, 046103 (2003).
[15] G. Kresse and J. Furthmüller, Phys. Rev. B **54**, 11169 (1996).
[16] A. S. Foster *et al.*, Phys. Rev. Lett. **86**, 2373 (2001).
[17] J. V. Lauritsen *et al.*, Nanotechnology **17**, 3436 (2006).
[18] G. H. Enevoldsen *et al.*, Phys. Rev. B **76**, 205415 (2007).
[19] A. I. Livshits *et al.*, Phys. Rev. B **59**, 2436 (1999).
[20] J. A. Ball *et al.*, Solid State Sci. **10**, 717 (2008).
[21] G. Busca *et al.*, Langmuir **9**, 1492 (1993).
[22] V. Sepelak *et al.*, J. Alloys Compd. **434-435**, 776 (2007).